Experimental Investigation of Flow Control over an Ahmed Body using DBD Plasma Actuator

S. Shadmani[1], S. M. Mousavi Nainiyan[1†], M. Mirzaei[2], R. Ghasemiasl[1] and S. G. Pouryoussefi[2]

[1] *Department of Mechanical Engineering, West Tehran Branch, Islamic Azad University, Tehran, Iran*
[2] *Department of Aerospace Engineering, K. N. Toosi University of Technology, Tehran, Iran*

†*Corresponding Author Email: mousavi.mojtaba@wtiau.ac.ir*

ABSTRACT

Ahmed body is a standard configuration of road vehicles and most of the studies of automobile aerodynamics are performed based on it. In this paper, the plasma actuator was used as an active flow control method to control the flow around the rear part of the Ahmed body with the rear slant angle of 25°. Experiments were carried out in a wind tunnel at two different velocities of U=10m/s and U=20m/s using steady and unsteady excitations. The hot-wire anemometer was used to measure the vortex shedding frequency at the downstream of the body. Pressure distribution was measured using 52 sensors and total drag force was extracted with a load cell. Furthermore, smoke flow visualization was employed to investigate the flow pattern around the body. The results showed that the plasma actuator was more effective on the pressure distribution and total drag force at the velocity of U=10m/s. In fact, by applying steady and unsteady excitations there was 7.3% and 5% drag reduction; respectively. While at the velocity of U=20m/s; the actuator had no significant effect on pressure distribution and total drag. As a remarkable result, the plasma actuator, especially in the steady actuation, has demonstrated its effectiveness on dispersing the longitudinal vortices and suppressing the separated flow on the rear slant at low velocities.

Keywords: Automotive; Aerodynamics; Wind tunnel; Drag reduction.

NOMENCLATURE

A	effective frontal area	P_∞	static pressure of free flow
AC	altering current	P_p	power of plasma actuator
C_p	pressure coefficient	pp	pick to pick
C_D	drag coefficient	Re	Reynolds number
D	drag force	$TRMS$	True Root Mean Square
H	model height	U	free stream velocity
In	induced	W	model width
L	model length	ρ	density
P	*pressure on the surface*		

1. INTRODUCTION

In recent years, by increasing the number of road transportation vehicles and consequently high fossil fuel consumption, the level of air pollution has raised to an alert situation in many metropolises (International Energy Agency 2007). In this regard, considering the international policies for reducing the consumption of fuels, the importance of the aerodynamics has been highlighted to minimize the resisting force of air flow. The lower amount of this force (known as drag force), causes lower fuel consumption and consequently the lower pollutant emissions (Hucho 1998).

Since the experimental study of flow control over different car models is expensive and time-consuming, normally a standard model is used as a sample of all car models. Experimental tests are carried out on the standard model and results will be applied for designing real cars. A standard model known as Ahmed body (Ahmed *et al.* 1984) which flow over it simulates three-dimensional flow pattern around an actual car due to its rear slant angle is popular in this regard. In some of the

researches carried out on the rear part of the model, flow pattern was investigated by changing the rear slant angle (Tunay *et al.* 2014; Strachan *et al.* 2007; Vino *et al.* 2005; Tunay *et al.* 2016). The results of these studies showed that the flow pattern can be considered two-dimensional for $\alpha < 12.5°$, and the drag force is independent of the angle variations (Strachan *et al.* 2007). For slant angles of $12.5°<\alpha<30°$, the drag force increases with increasing the angle and the flow pattern is 3-dimensional (Fig. 1). The drag force reaches its maximum value at $\alpha=25°$ (Fig. 2) (Vino *et al.* 2005). For $\alpha>30°$, the flow is totally separated and the drag force is independent of the angle (Tunay *et al.* 2016). Therefore, the flow regimes in the first and third α-ranges are similar and fall within low-drag zones. However, due to the three-dimensional flow, the second α-range ($12.5°<\alpha<30°$) is known as high-drag zone (Fig. 2).

In other works, active and passive flow controls were adopted in the tailing section of the model in an attempt to modify the flow in this region and reduce the drag force. Installation of various types of deflectors (Hanfeng *et al.* 2016; Fourrie *et al.* 2011) is among the passive flow control methods which require no external energy (Hanfeng *et al.* 2016). One of the drawbacks of these methods is that they have uncontrolled performance for various conditions (Kourta *et al.* 2012). On the other hand, active control methods such as mixed jets (Kourta *et al.* 2012), pulse jets (Joseph *et al.* 2012) and fluidic oscillators (Metka *et al.* 2015) have been investigated. Controllable nature of these methods allow them to be turned on/off on demand. Results of these methods in terms of reducing the drag force applied to Ahmed model are given in Table 1.

Dielectric barrier discharge (DBD) plasma actuator is another modern tool for active flow control which has been used in aviation applications. Figure 3 depicts the plasma actuator mechanism. It consists of two electrodes separated by a dielectric barrier, whereby air molecules above the insulated electrode are ionized by establishing a strong electric field. This ionized gas which is called plasma extends from the edge of the upper exposed electrode to the trailing edge of the lower insulated electrode. This adds up local momentum to the flow passing above the region as moving charged particles collide with other neutral particles of the gas surrounded the actuator (He *et al.* 2007).

These actuators have many applications including separation control on leading edge of airfoils (Post and Corke 2004; Benard *et al.* 2008; Puoryoussefi *et al.* 2016), dynamic stall control of airfoils (Post and Corke 2006), flow control on bluff bodies (Do *et al.* 2007; Thomas *et al.* 2008; Thomas *et al.* 2005; Rizzetta and Visbal 2008; Gregory *et al.* 2008), flow control on boundary layer (Schatzman and Thomas 2008; Baughn *et al.* 2006; Font 2006), lifting applications (Corke *et al.* 2004), and flow control in turbomachines (Huang *et al.* 2006; Vanness *et al.* 2006). Boucinha *et al.* (2011) installed three groups of plasma actuators on the rear slant of an Ahmed body to investigate only the drag reduction on the

model at velocity of 10m/s. They showed that the use of these actuators can reduce the drag force up to 8% by adopting the actuators on the upper part of the surface. Moreover, Khalighi *et al.* (2016) installed plasma actuators on the four edges of an Ahmed body model with 0° rear slant angle to analyze passing flow from the trailing part of the model. They showed the drag force decreases up to 21.4% at 10m/s.

In the present work, effects of plasma actuator system for flow control around an Ahmed body is experimentally studied in a wind tunnel using pressure distribution, drag force measurement and flow visualization. Experiments were performed at Reynolds numbers of Re=4.5×105 and Re=9×105 (based on model length of 0.67m and free flow velocities of U=10m/s and U=20m/s, respectively), with the rear slant angle of 25° to have a dominant three-dimensional flow pattern and highest drag force (Fig. 2). Moreover, measurements of the natural frequency of vortex shedding, unsteady actuation, and flow control capabilities were compared for steady and unsteady actuations. In previous researches using all these methods and conditions has not been reported. It should be noted that the plasma actuator installation position may correspond to trailing edge of the roof, trunk edge, or below rear bumper of a vehicle.
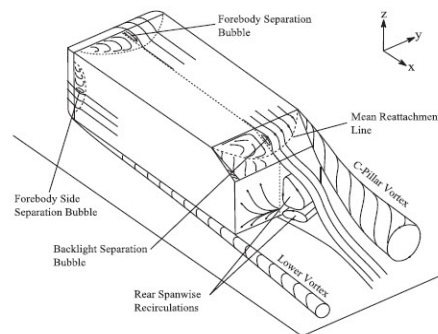

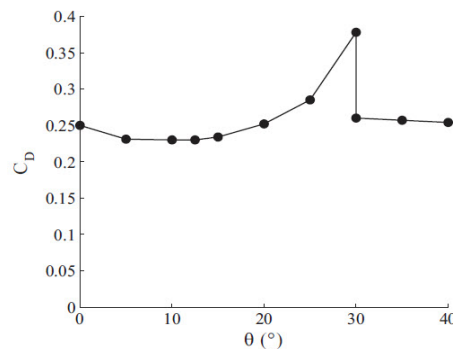**Fig. 1. Flow pattern behind Ahmed body model at the rear slant angle of 25° (Ahmed *et al*. 1984).**

Fig. 2. Plot of drag coefficient vs. slant angle (Ahmed *et al*. 1984).

2. EXPERIMENTAL DETAILS

Experiments were performed in an open loop low-speed wind tunnel at K. N. Toosi University (Iran) with a test section of $1×1.2m^2$ and length of 3m (Fig. 4). Turbulence intensity of the flow was below

0.2% and non-uniformity of the flow along the test section was about ±5%.

2.1 Model Description

The model was cons built of 6mm-thick Plexiglas at 64% of the full scale original model. As mentioned before, in order to establish three-dimensional flow behind the model and maximize the drag force, the rear slant angle was 25°. Figure 5 shows the details of the model. The blockage ratio of the model in the test section is 3.8%.

In order to eliminate the wall effects on the bottom of the wind tunnel (Hucho and Sovran 1993), the model was mounted on a rectangular surface at given spacing (Fig. 6). The distance between surface and tunnel floor was 16×10-2m, with the model connected to the surface via four cylindrical supports with the diameter of 2×10-2m and height of 32×10-2m. Moreover, leading edge of the surface was designed sharply to minimize the thickness of the developed boundary layer (Fig. 7). The thickness of the boundary layer formed on the surface at flow velocities of 10 to 50 m/s was about 1.5×10-2m (Joseph *et al.* 2012) so that the boundary layer on the surface has no effect on the model.

2.2 Instruments and Measurement Techniques

Pressure distribution was obtained using 52 pressure sensors (pressure transducers) installed only on half of the slant and vertical surfaces of the model due to symmetry. The arrangement of the sensors is demonstrated in Fig. 8. Each sensor consists of a tube of outer and inner diameters of 4mm and 2mm respectively. The pressure sensors were connected to a 28-channel pressure transducer apparatus (Honeywell-DC005NDC4). The results were monitored on a computer using an A/D (PCI6224) board, Lab View software, and pressure distribution software. Sampling interval was set to 5 second and pressure coefficients were calculated using the Eq. (1):

$$C_p = \frac{P - P_\infty}{0.5 \times \rho \times U^2} \tag{1}$$

Where P is pressure on the surface, P_∞ is the static pressure of free stream, U_∞ is the velocity of free stream, and ρ is air density in the environment. The uncertainty of the measurement device is about ±0.01.

The drag force was determined using a load cell. In order to minimize friction force between the model and lower surface, the model was positioned on two rows of rails and wagons (Fig. 9a), and according to Fig. 9b, attaching a light aluminum rod of 0.5 m which was attached to load cell at ±1gr accuracy on the other end.

In order to find natural frequency of vortex shedding behind the model, Hot-wire anemometer system was utilized (Fig. 10). The Hot-wire probe could be displaced along x and y directions with a traverse mechanism.

Table 1 Results of the research on the reduction of drag force.

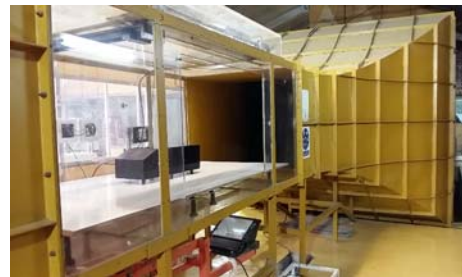| Studies	Reynolds Number	Drag Reduction (%)
Hanfeng *et al.* 2016	8.7×10^5	9.3-10.7
Fourrie *et al.* 2011	3.1-7.7×10^5	9
Kourtaa *et al.* 2012	1.2×10^6	6.5-8.5
Joseph *et al.* 2012	1.4×10^6	6-8
Metka *et al.* 2015	1.4×10^6	7.5

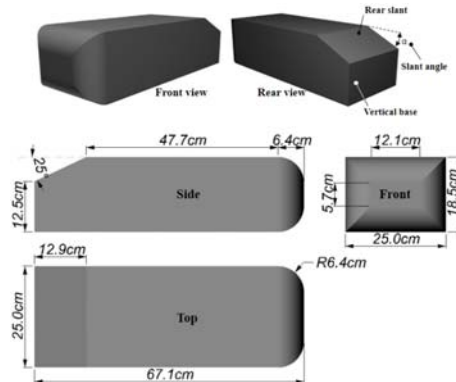**Fig. 4. The used wind tunnel in this research.**

Fig. 5. Three-dimensional view of Ahmed model and model dimensions (mm).
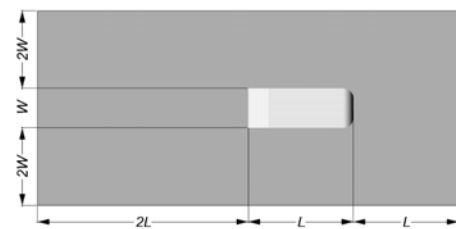

Fig. 6. Model position on the surface.

Fig. 7. View of the leading edge of the table which is designed sharply.

2.3 Plasma Actuator System

The input voltage to the plasma actuator was supplied by a high-voltage AC with the sinusoidal carrier wave and maximum output power of 1000W. Two digital multimeter sets were used to check out

actuation and carrier frequencies. The duty cycle and applied voltage were monitored by an oscilloscope. Furthermore, a digital multimeter (True RMS) was used to measure the mean electric current (Fig. 11).

According to Fig. 12, the plasma actuator mounted such that, the exposed electrode was installed on the trailing edge of the upper surface, while the covered electrode was placed on the leading edge of the slant, in an edge-to-edge arrangement. The electrodes were made of copper, with the thickness of 50microns. The length of the electrodes was equal to the model width, 25cm, with the widths of the exposed and covered electrodes of 5 and 15mm, respectively. In all arrangements, plasma actuator dielectric was composed of six layers of Kapton adhesive at the breakdown voltage of 7kV/mm and dielectric constant of 3.4.

For a quiescent flow, installing a plasma actuator on a flat surface, a digital manometer (Testo 0560 5126) along with a silicon micro-tube were applied to determine maximum induced velocity versus the applied voltage, V_{pp} (pick-to-pick). The corresponding voltage was constant in all experiments. Other electrical parameters including carrier frequency (f_{AC}), was set to 10kHz, and actuation frequency, was determined based on the natural frequency of vortex shedding behind the model. Moreover, the actuator acted at steady and unsteady excitations, and duty cycle in unsteady actuation was 50%.

3. RESULTS AND DISCUSSION

3.1 Quiescent Flow Test

In the first experiment, the maximum induced velocity in quiescent conditions was measured. Here we tried to reach the appropriate carrier voltage to reach the maximum induced velocity. The results are depicted in Fig. 13. It can be seen that the mean velocity occurs at 6kV. The induced velocity reached a maximum of 6m/s and then dropped down with further increase in voltage. This indicates that, with increasing the applied voltage to overcharged state, the plasma actuator becomes saturated, thereby changing the plasma regime from uniform mode (Fig. 14a) to stratified mode (Fig. 14b).

In this situation, due to high conductivity, plasma is discharged at the higher density, reducing plasma density outside the region. This eventually leads to
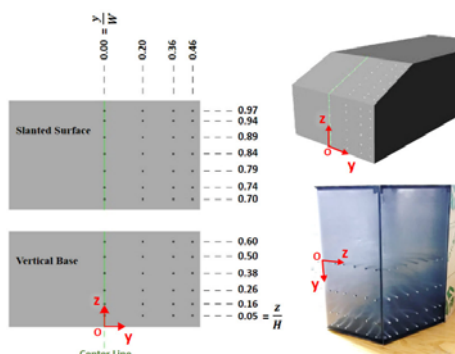
the reduction of induced velocity and this reduces actuator body force (Pouryoussefi *et al*. 2015; Dalvand *et al*. 2018).

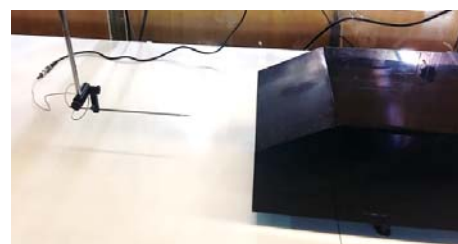**Fig. 9. a) Rail and wagon mechanism and; b) Load cell mechanism to measure drag force.**

Fig. 10. View of the position of Hot-wire probe behind the model.
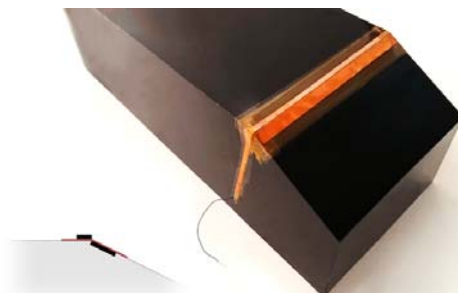

Fig. 11. Measurement devices.

Fig. 12. The position of plasma electrodes.

3.2 Hot-Wire Measurement

A proper carrier frequency in unsteady excitation is estimated using vortex shedding frequency. In most of the time, this frequency is set to be equal with the shedding frequency (Pouryoussefi *et al.* 2015). For this purpose, 1-D Hot-wire probe was placed at the three different locations behind the model shown in Fig. 15.

Figures 16-17 show spectral analysis of hot-wire

Fig. 8. The position of pressure sensors.

signal (effective instantaneous velocity) at (X^*=0.5, Y^*=0.6) position to demonstrate variations of velocity at the natural frequency of vortex shedding. At U=10m/s and U=20m/s, dominant frequencies of vortex shedding (peak of the curve) were about 20Hz and 40Hz, respectively. Therefore, the dimensionless Strouhal number would be equal to 0.37 at both velocities, which is in good agreement with other works reported in Table 2. Strouhal number is calculated based on Eq. (2):

$$St = \frac{f \times H}{U} \qquad (2)$$

Where H is the model height, f is natural frequency of back-model vortices, and U is free stream velocity.

Considering the results obtained in this section and the section 3-1, the input electrical parameters which are used in all experiments and also the power consumption of the plasma actuator are presented in Table 3. The power of plasma actuator is calculated according to the research work of Pouryoussefi *et al.* (2016) as Eq. (3):

$$P_P = \frac{V_{PP}}{2\sqrt{2}} \times I_{RMS} \times \cos\phi \qquad (3)$$

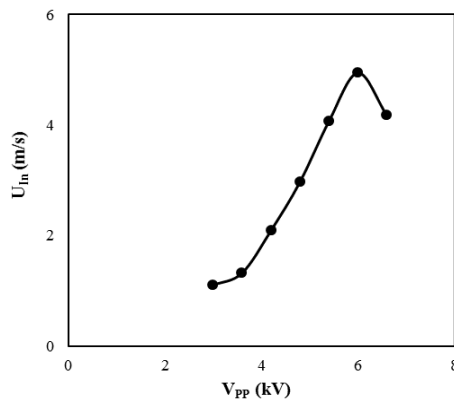Where I_{RMS} is ampere, V_{PP} is pick to pick voltage and φ is about 6 ° (Pouryoussefi *et al.* 2016).

Fig. 13. Plot of induced velocity by plasma actuator, U_{In} (induced flow) based on The applied voltage, V_{pp} (pick-to-pick).
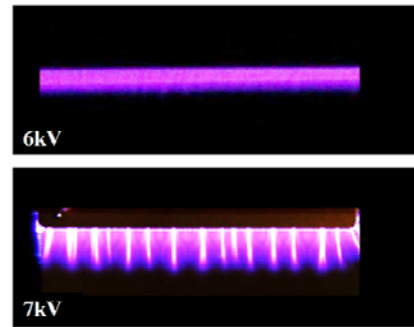

Fig. 14. a) Uniform plasma distribution regime and; b) stratified plasma distribution regime
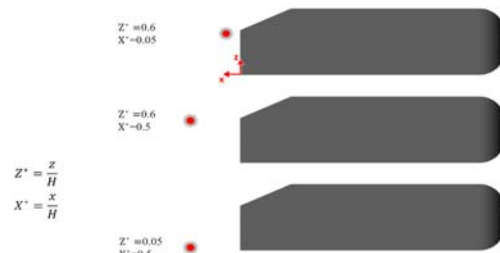

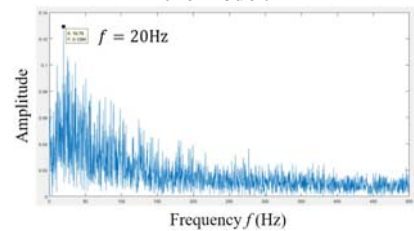**Fig. 15. Position of 1-D Hot-wire probe behind the model.**

Fig. 16. Plot of frequency and amplitude of the vortexes behind the model at the velocity of 10m/s.
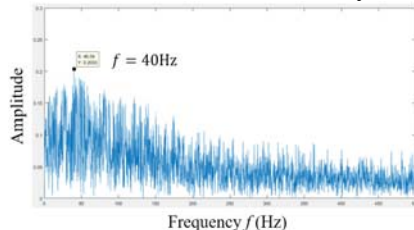

Fig. 17. Plot of frequency and amplitude of the vortexes behind the model at the velocity of 20m/s.

Table 2 Comparison between the obtained Strouhal number in this research and other research works.

Studies	Reynolds number	Type of study	Based on	Strouhal number
Minguez *et al.* (2008)	7.7×10^5	Numerical (LES)	Model height	0.42
Ceyrowsky *et al.* (2009)	7.7×10^5	Numerical (URANS)	Model height	0.5
Joseph *et al.* (2012)	3.9-7.7×10^5	Experimental (Hot-Wire)	Vertical Based height	0.31
Present Study	4.5-9×10^5	Experimental (Hot-Wire)	Model height	0.37

Table 3 Input electrical parameters of plasma actuator.

No.	Velocity U (m/s)	Type	Carrier Frequency f_{AC} (kHz)	Voltage V_{PP} (kV)	Ampere I_{TRMS} (mA)	Power Consumption P_P (W/cm)	Duty Cycle (%)	Excitation Frequency (Hz)
1	10	Steady	10	6	28.6	2.41	100	-
2	10	Unsteady	10	6	20.2	1.70	50	20
3	20	Steady	10	6	28.6	2.41	100	-
4	20	Unsteady	10	6	20.2	1.70	50	40

3.3 Pressure Distribution

Pressure distribution difference between the front and rear of the model leads to pressure drag force. Krajnovic and Davidson (2005) showed that the contribution of pressure drag (Form drag) is about 80% of total drag. This necessitates obtaining the pattern of pressure variations across two end surfaces of the model to investigate the effect of flow across the region. Figure 18 shows pressure coefficients contours on the slant surface behind the model at U=10m/s (Re=4.5×10^5) and U=20m/s (Re=9×10^5), which is good in agreement with the results reported by Keogh *et al.* (2016), Lienhart *et al.* (2003) and Joseph *et al.* (2012) for no actuator conditions (Fig. 19).

According to Fig. 18, low-pressure regions of the flow extend along leading edge of the slant so that one can stipulate, separation bubble and flow jump over the leading edge of slant have occurred in such regions (see Fig. 1). Moving toward central areas, the low-pressure zones are gradually replaced by higher pressure, i.e. the pressure is recovered. At the lateral edges, low-pressure are developed on the surface, this indicates the isolation of C-pillar vortexes from the top corner of the surface along the surface length (see fig. 1).

It can be observed in Fig. 20, by applying plasma actuation at the velocity of U=10m/s, the volume of the low-pressure zones on the leading edge of the surface reduced considerably, such that the region was completely disappeared in steady state actuation. This indicates that by actuating the plasma, the developed vortex is degraded and the separated flow tends to attach to the surface. This will be observed in visualization tests as well. Moreover, reduction of low-pressure zones in the lateral edges of the surface is assign of the reduced effect of C-pillar longitudinal vortexes behind the model. The effect of steady actuation can be seen more significant than that of unsteady one.

According to Fig. 21, at the velocity of U=20m/s, plasma actuation imposed no significant effect on the reduction of low-pressure regions developed by the vortices behind the model, such that nearly the same pressure distribution is obtained for the steady and unsteady actuations.

Figure 22 shows the comparison between pressure distribution of no-actuation, steady actuation, and unsteady actuation conditions on the centerline of the model at velocities of 10m/s and 20m/s. At the velocity of 10m/s, plasma actuation has resulted in considerable rising pressure coefficients, particularly across the regions at the slant while the effect of plasma actuator is insignificant at the velocity of 20m/s.
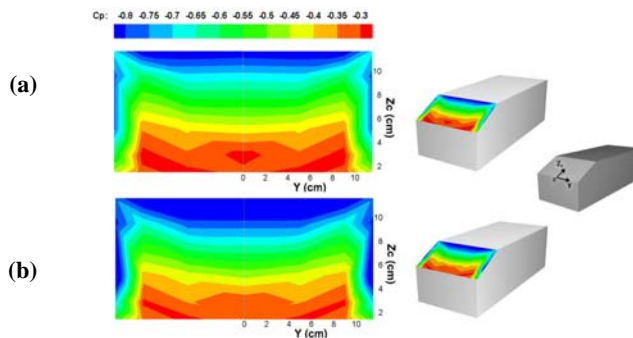

Fig. 18. Contours of pressure distribution on the rear slant of an Ahmed body in plasma off mode at velocities of a) 10m/s and; b) 20m/s.
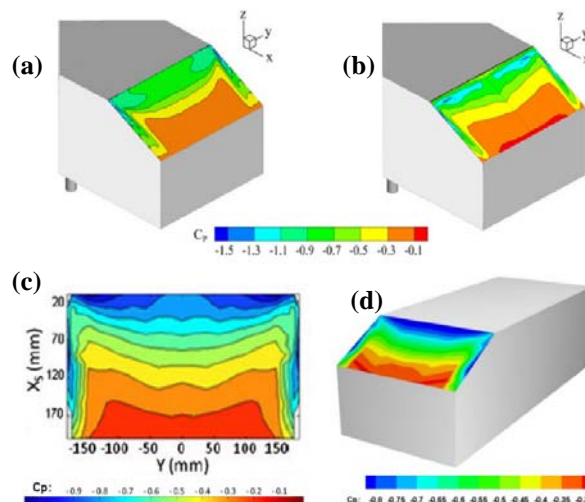

Fig. 19. Contours of pressure distribution on the rear slant of the Ahmed model in velocity of 20m/s and no actuation condition in the studies of a) Keogh *et al.* (2016); b) Lienhart *et al.* (2003); c) Joseph *et al.* (2012) and; d) Present study.

Fig. 20. Contours of pressure coefficient distribution on the rear slant of Ahmed body at the velocity of 10m/s in a) Plasma off; b) Steady actuation and; c) Unsteady actuation.
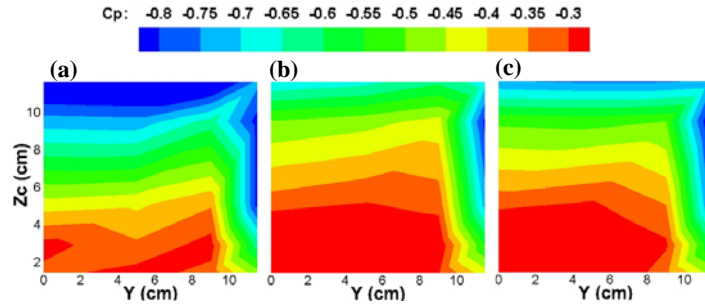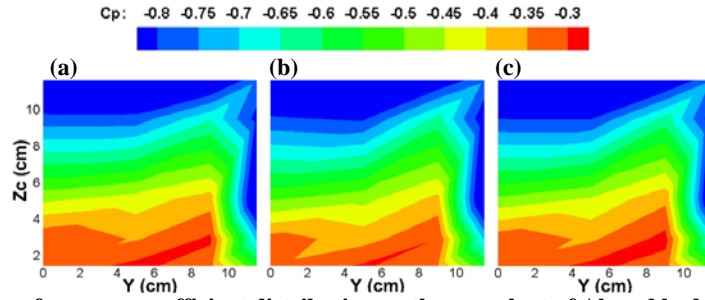

Fig. 21. Contours of pressure coefficient distribution on the rear slant of Ahmed body at the velocity of 20m/s in a) Plasma off; b) Steady actuation and; c) Unsteady actuation.
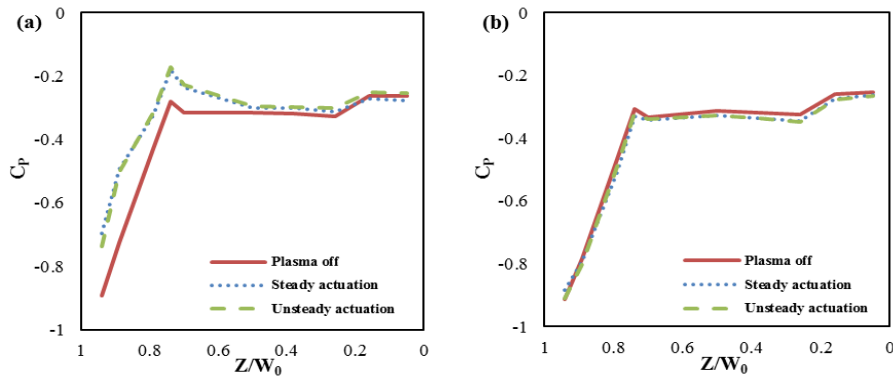

Fig. 22. Plot of pressure coefficient distribution on the centerline of the model at a) U=10m/s and; b) U=20m/s.

3.4 Drag Measurement

In the present research, total drag force was measured using a load cell. For no plasma actuation, the drag force was found to be 0.8N at Re=4.5×105 (U=10m/s) and 3.22N at Re=9×105 (U=20m/s). Since drag force is directly proportional to the velocity squared, it can be observed that doubling the velocity, leads to four times higher drag force. According to the drag force coefficient (Eq. (4)):

$$C_d = \frac{F_D}{0.5 \times \rho \times A \times U^2} \tag{4}$$

Where *U* is free flow (stream) velocity, *A* is the effective frontal area, and *ρ* is air density.

The drag coefficient of the model was found to be 0.29, which is in good agreement with the results reported by Ahmed *et al.* 1984 (see Fig. 2).

Based on Fig. 23, applying plasma actuation at the

velocity of 10m/s, the values of drag force reduced about 7.3% and 4.88% in steady and unsteady actuations, respectively. While, at the velocity of 20m/s, the reduction of drag force in steady and unsteady actuations reached 2.13% and 1.5%, respectively. The results indicate that, at lower velocities, particularly in steady actuation, the plasma actuator can reduce overall drag force more effective. Considering the fact that, the dominant drag force in the Ahmed model is pressure drag (Krajnovic and Davidson 2005b), the results obtained from drag force measurement using load cell shows good agreement with the pressure measurement results.

3.5 Flow Visualization

Since the plasma actuator was more effective at 10m/s, for flow visualization study we only conducted our experiment at this velocity. According to Fig. 24 a, in plasma off mode, the airflow separates from the surface as it passes over the leading edge of the rear slant, developing a

vortex on the slant surface. Moreover, within the flow passing through the lower part of the model, a larger vortex is formed behind the vertical surface. Figures 24b and 24c show that the plasma actuator suppresses the flow passing over the surface edge by actuating shear layer, and the separated flow from the slant surface gets closer to the surface. As a result, the developed vortex on the slant is degraded and the volume of the wake formed behind the vertical surface is reduced. This lead reduction in pressure drag (Form drag) (Section 3.4).
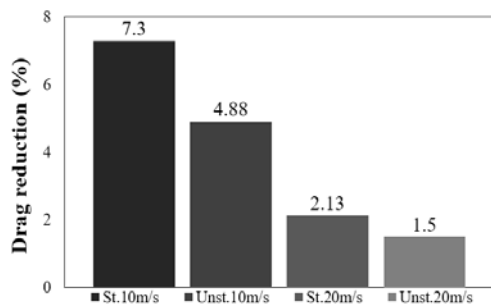

Fig. 23. Plot of drag reduction
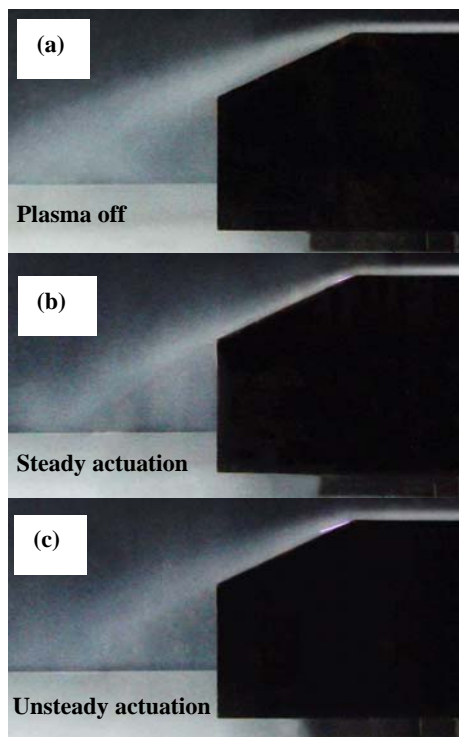**(St: Steady actuation, Unst: Unsteady actuation).**

Fig. 24. Pattern of the flow passing through the
region behind the model at U=10m/s in:
a) Plasma off; b) Steady actuation and;
c) Unsteady actuation.

4. CONCLUSIONS

In the present research, the plasma actuator was used to control flow over an Ahmed body model with a rear slant angle of 25°. Plasma actuator electrodes were installed on the leading edge of the slant behind the model, and actuations were performed in steady and unsteady excitations at different Reynolds numbers with flow velocities of U=10m/s and U=20m/s.

In quiescent flow test, using the plasma actuator on a flat surface, the appropriate applied voltage was determined based on maximum induced velocity. Also, actuation frequency of the plasma actuator was obtained by measuring natural frequency of the vortex shedding behind the model at U=10m/s and U=20m/s velocities.

Visualization results indicate that at U=10m/s the plasma actuator is capable of suppressing the separated flow from the leading edge of the rear slant and attaching the flow back to the surface by actuating the shear layer. For this case, the volume of longitudinal vortices behind the model is reduced while increasing pressure coefficient on the slant at the same time. By reduction of the pressure difference between front and rear part of the model, pressure drag force and hence total drag force decreases, so that the reduction of drag force in steady and unsteady excitations was 7.3% and 4.88%, respectively. At the velocity of U=20m/s, the results indicated that the plasma actuator is not effective on pressure enhancement on the rear part of the model and the reduction of drag force in both steady and unsteady excitations is about 2%. Therefore, application of the plasma actuator at low velocities, particularly in steady excitation, can serve as an effective tool for flow control and drag reduction.

For further investigation of plasma actuator effectiveness, it is suggested to use several plasma actuators in different positions of the model simultaneously and evaluate the relationship between the plasma actuator energy consumption and the amount of fuel reduction caused by the drag force reduction evaluated.

REFERENCES

Ahmed, S. R., G. Ramm, and G. Faitin (1984). Some salient features of the time-averaged ground vehicle wake. *SAE Technical Paper 840300*.

Baughn, J. W., C. Porter, B. L. Peterson, T. E. McLaughlin, C. L. Enloe, G. I. Font, and C. Baird (2006). Momentum Transfer for an Aerodynamic Plasma Actuator with an Imposed Boundary Layer. *44th AIAA aerospace sciences meeting. AIAA* 2006-168.

Benard, N., P. Braud, and J. Jolibois (2008). Airflow Reattachment Along a NACA 0015 Airfoil by Surface SDBD Actuator-Time Resolved PIV Investigation. *AIAA Paper* 2008-4202.

Boucinha, V., R. Weber, and A. Kourta (2011). Drag reduction of a 3D bluff body using plasma actuators. *International Journal of Aerodynamics* 1, 262-281.

Ceyrowsky, T., C. Brucker, and R. Schwarze (2009). Unsteady RANS Simulations of Flows Around a Simplified Car Body. *EUROMECH Colloquium 509 Vehicle Aerodynamics External Aerodynamics of Railway Vehicles, Trucks,*

Buses and Cars, Berlin, Germany.

Corke, T. C., C. He, and M. Patel (2004). Plasma Flaps and Slats: An Application of Weakly-Ionized Plasma Actuators. *AIAA Paper* 2004-2127.

Dalvand, E., S. M. Ebrahimi, and S. G. Pouryoussefi (2018). Experimental investigation, modeling and prediction of transition from uniform discharge to filamentary discharge in DBD plasma actuators using artificial neural network. *Applied Thermal Engineering* 129, 50-61.

Do, H., W. Kim, M. O. Mungal, and M. A. Cappelli (2007). Bluff Body Flow Separation Control Using Surface Dielectric Barrier Discharges. *AIAA Paper* 2007-939.

Font, G. I. (2006). Boundary Layer Control with Atmospheric Plasma Discharges. *AIAA Journal* 44, 1572-1578.

Fourrie, G., L. Keirsbulck, L. Labraga, and P. Gilliéron (2011). Bluff-body drag reduction using a deflector. *Experiments in Fluids* 50 (2), 385–395.

Gregory, J., C. Porter, D. Sherman, and T. McLaughlin (2008). Circular Cylinder Wake Control Using Spatially Distributed Plasma Forcing. *AIAA Paper* 2008-4198.

Hanfeng, W., Z. Yu, Z. Chao, and H. Xuhui (2016). Aerodynamic drag reduction of an Ahmed body based on deflectors. *Journal of Wind Engineering and Industrial Aerodynamics* 148, 34–44.

He, C., T. C. Corke, and M. P. Patel (2007). Numerical and Experimental Analysis of Plasma Flow Control Over a Hump Model. 45th Aerospace Sciences Meeting. *AIAA paper* 2007-0935.

Huang, J., T. C. Corke, and F. O. Thomas (2006). Plasma Actuators for Separation Control of Low-Pressure Turbine Blades. *AIAA Journal.*

Hucho, W. H., and G. Sovran (1993). Aerodynamic of Road Vehicles. *Annual Reviews Fluid Mechanics* 25, 485-537.

Hucho, W. H. (1998). Aerodynamic of road vehicles. *Cambridge University Press*, Cambridge, England. World energy outlook 2007 China and India insights (executive summary), *International Energy Agency (IEA).*

Joseph, P., X. Amandolese, and J. Aider (2012). Drag reduction on the 25° slant angle Ahmed reference body using pulsed jets. *Experiments in Fluids* 52, 1169–1185.

Khalighi, B., J. Ho, J. Cooney, B. Neiswander, and T. Han (2016). Aerodynamic Drag Reduction Investigation for A Simplified Road Vehicle Using Plasma Flow Control. *Proceedings of the ASME 2016 Fluids Engineering Division Summer Meeting,* FEDSM 2016-7927.

Kourta, A., and C. Leclerc (2012). Characterization of synthetic jet actuation with application to Ahmed body wake. *Sensors and Actuators A* 192, 13-26.

Krajnovic, S., and L. Davidson (2005b). Flow around a simplified car, Part 2: Understanding the Flow. *Journal of Fluids Engineering* 127, 919–928.

Keogh, J., T. Barber, S. Diasinos, and G. Doig (2016). The aerodynamic effects on a cornering Ahmed body. *Journal of Wind Engineering and Industrial Aerodynamics* 154, 34–46.

Lienhart, H., and S. Becker (2003). Flow and Turbulence Structure in The Wake of a Simplified Car Model. *SAE Technical Paper.*

Metka, M., and J. W. Gregory (2015). Drag Reduction on the 25-deg Ahmed Model Using Fluidic Oscillators. *Journal of Fluids Engineering ASME.*

Minguez, M., R. Pasquetti R, and E. Serre (2008). High-Order Large-Eddy Simulation of Flow Over The "Ahmed Body" Car Model. *Physics of Fluids* 20, 095-101.

Post, M. L., and T. C. Corke (2004). Separation Control on a High Angle of Attack Airfoil Using Plasma Actuators. AIAA *Journal.*

Post, M. L., and T. C. Corke (2006). Separation Control Using Plasma Actuators-Dynamic Stall Vortex Control on an Oscillating Airfoil. *AIAA Journal.*

Pouryoussefi, S. G., M. Mirzaei, and M. Hajipour (2015). Experimental Study of Separation Bubble Behind a Backward-Facing Step Using Plasma Actuator. *Acta Mechanica* 226, 1153-1165.

Puoryoussefi, S. G., M. Mirzaei, F. Alinejad, and S. M. Puoryoussefi (2016). Experimental investigation of separation bubble control on an iced airfoil using plasma actuator. *Applied Thermal Engineering* 100, 1334-1341.

Rizzetta, D., and M. Visbal (2008). Large-Eddy Simulation of Plasma-Based Control Strategies for Bluff Body Flow. *AIAA Paper* 2008-4197.

Schatzman, D., and F. O. Thomas (2008). Turbulent Boundary Layer Separation Control Using Plasma Actuators. *AIAA Paper* 2008-4199.

Strachan, R., K. Knowles, and N. Lawson (2007). The vortex structure behind an Ahmed reference model in the presence of a moving ground plane. *Experiments in Fluids* 42, 659–669.

Thomas, F. O., A. Kozlov, and T. C. Corke (2005). Plasma Actuators for Landing Gear Noise Control. *AIAA Paper* 2005-3010.

Thomas, F. O., A. Kozlov, and T. C. Corke (2008). Plasma Actuators for Cylinder Flow Control and Noise Reduction. *AIAA Journal.*

Tunay, T., B. Sahin, and V. Ozbolat (2014). Effects of rear slant angles on the flow characteristics of Ahmed body. *Experimental Thermal and Fluid Science* 57, 165–176.

Tunay, T., B. Yaniktepe, and B. Sahin (2016). Computational and experimental investigations

of the vortical flow structures in the near wake region downstream of the Ahmed vehicle model. *Journal of Wind Engineering and Industrial Aerodynamics* 159, 48–64.

Vanness, D. K., T. C. Corke, and S. C. Morris (2006). Turbine Tip Clearance Flow Control

Using Plasma Actuators. *AIAA Paper* 2006-0021.

Vino, G., S. Watkins, P. Mousley, J. Watmuff, and S. Prasad (2005). Flow structures in the near-wake of the Ahmed model. *Journal of Fluids Structure* 20, 673–69.